J Therm Anal Calorim (2011) 103:805–812
DOI 10.1007/s10973-010-1057-5

Kinetics and thermodynamics of thermal decomposition of $NH_4NiPO_4 \cdot 6H_2O$

Xuehang Wu · Wenwei Wu · Shushu Li · Xuemin Cui · Sen Liao

Received: 23 July 2010 / Accepted: 14 September 2010 / Published online: 7 October 2010

Abstract The single phase $NH_4NiPO_4 \cdot 6H_2O$ was synthesized by solid-state reaction at room temperature using $NiSO_4 \cdot 6H_2O$ and $(NH_4)_3PO_4 \cdot 3H_2O$ as raw materials. XRD analysis showed that $NH_4NiPO_4 \cdot 6H_2O$ was a compound with orthorhombic structure. The thermal process of $NH_4NiPO_4 \cdot 6H_2O$ experienced three steps, which involves the dehydration of the five crystal water molecules at first, and then deamination, dehydration of the one crystal water, intramolecular dehydration of the protonated phosphate groups together, at last crystallization of $Ni_2P_2O_7$. In the DTA curve, the two endothermic peaks and an exothermic peak, respectively, corresponding to the first two steps' mass loss of $NH_4NiPO_4 \cdot 6H_2O$ and crystallization of $Ni_2P_2O_7$. Based on Flynn–Wall–Ozawa equation, and Kissinger equation, the average values of the activation energies associated with the thermal decomposition of $NH_4NiPO_4 \cdot 6H_2O$, and crystallization of $Ni_2P_2O_7$ were determined to be 47.81, 90.18, and 640.09 kJ mol^{-1}, respectively. Dehydration of the five crystal water molecules of $NH_4NiPO_4 \cdot 6H_2O$, and deamination, dehydration of the crystal water of $NH_4NiPO_4 \cdot H_2O$, intramolecular dehydration of the protonated phosphate group from $NiHPO_4$ together could be multi-step reaction mechanisms. Besides, the thermodynamic parameters ($\Delta H^{\neq}$, $\Delta G^{\neq}$, and $\Delta S^{\neq}$) of the decomposition reaction of $NH_4NiPO_4 \cdot 6H_2O$ were determined.

Keywords $NH_4NiPO_4 \cdot 6H_2O$ · Non-isothermal kinetics · Thermodynamics · Thermal decomposition · Solid-state reaction at room temperature

X. Wu · W. Wu (✉) · S. Li · X. Cui · S. Liao
School of Chemistry and Chemical Engineering, Guangxi University, Nanning 530004, China
e-mail: gxuwuwenwei@yahoo.com.cn

Introduction

The synthesis and structural characterization of nickel (II) phosphates have received considerable amount of attention due to diversity of structure types and abundance of nickel (II) phosphate framework compounds as well as to their potential applications as new materials that may have ion exchange, ionic conductivity, and interesting magnetic properties [1]. Nickel (II) phosphates occur in many forms: such as $Ni_3(PO_4)_2 \cdot 8H_2O$ [2], $NH_4NiPO_4 \cdot H_2O$, $KNiPO_4 \cdot H_2O$, and $NH_4NiPO_4 \cdot 6H_2O$, etc. The choice of synthetic method and raw materials is important, as it can lead to the production of several phases with predetermined structure types [1]. Ammonium phosphates of general formula $NH_4M^{II}PO_4 \cdot H_2O$ were first described in 1864 by Debray. The series of nickel (II) phosphates $M^{I}NiPO_4 \cdot H_2O$ (M^{I} = K, NH_4) were reported by Bassett and Bedwell in 1933 [3]. Infrared spectroscopic measurements [4] showed that the ammonium compounds contained coordinated water and ammonium ions, instead of having the alternative composition $NiHPO_4NH_3 \cdot H_2O$. Carling et al. [5] obtained $NH_4NiPO_4 \cdot H_2O$ by precipitation from aqueous solution using a method derived from that of Bassett and Bedwell, and determined the crystal and magnetic structures of the compound. Aintzane et al. [1] prepared $NH_4NiPO_4 \cdot nH_2O$ ($n = 1$, 6) via direct precipitation method in which $NiCl_2 \cdot 6H_2O$ was used as the source of nickel (II), H_3PO_4 was used as the source of phosphorus, and NH_4OH was used as the source of ammonium, in which the presence of three different nickel (II) phosphates has been observed: $Ni_3(PO_4)_2 \cdot 8H_2O$, $NH_4NiPO_4 \cdot H_2O$, and $NH_4NiPO_4 \cdot 6H_2O$. Therefore, single phase nickel (II) phosphates can be obtained only with special attention to the control of the pH in the solvent medium, which was regulated by addition of NH_4OH.

The aim of this work is to prepare single phase $NH_4NiPO_4{\cdot}6H_2O$ via solid-state reaction at room temperature and to study the kinetics and thermodynamics of the decomposition of $NH_4NiPO_4{\cdot}6H_2O$ using TG-DTA technique. Non-isothermal kinetics of the decomposition process of $NH_4NiPO_4{\cdot}6H_2O$ was interpreted by Flynm–Wall–Ozawa (FWO) method [6, 7], and the Kissinger method [8]. The kinetic (E_a, A, mechanism) and thermodynamic parameters ($\Delta H^{\neq}$, $\Delta S^{\neq}$, $\Delta G^{\neq}$) of the decomposition reaction of $NH_4NiPO_4{\cdot}6H_2O$ are discussed for the first time.

Experimental

Reagent and apparatus

All chemicals were of reagent grade purity. TG/DTA measurements were made using a Netsch 40PC thermogravimetric analyzer. X-ray powder diffraction (XRD) was performed using a Rigaku D/max 2500 V diffractometer equipped with a graphite monochromator and a Cu target. The FT-IR spectra of the product and its products of thermal decomposition were recorded on a Nexus 470 Fourier transform IR (FT-IR) instrument. The morphology of the product and its calcined samples were examined by S-3400 scanning electron microscopy (SEM).

Preparation of $NH_4NiPO_4{\cdot}6H_2O$

The binary ammonium nickel phosphates $NH_4NiPO_4{\cdot}6H_2O$ were prepared by solid-state reaction at room temperature [3] using $NiSO_4{\cdot}6H_2O$ and $(NH_4)_3PO_4{\cdot}3H_2O$ as starting materials. In a typical synthesis, $NiSO_4{\cdot}6H_2O$ (27.21 g), $(NH_4)_3PO_4{\cdot}3H_2O$ (24.63 g), and surfactant polyethylene glycol (PEG)-400 (1.5 mL) were put in a mortar, and the mixture was fully ground by hand with a rubbing mallet for 40 min. The grinding velocity was about 90 circles/min, and the strength applied was moderate. The reactant mixture gradually became damp, and then a paste formed quickly. The reaction mixture was kept at room temperature for 4 h. The mixture was washed with deionized water to remove soluble inorganic salts until SO_4^{2-} ion could not be visually detected with a 0.5 mol L^{-1} $BaCl_2$ solution. The solid was then washed with a small amount of anhydrous ethanol and dried at 353 K for 3 h to give the single phase $NH_4NiPO_4{\cdot}6H_2O$.

Method of determining kinetic parameters

Determination of activation energy by FWO method [6, 7]

Kinetic equation of solid-state reaction can be expressed as Eq. 1:

$$\frac{d\alpha}{dt} = Ae^{-E_a/RT}f(\alpha) \tag{1}$$

When heating rate is kept fixed value, that is: $\beta = dT/dt$. Equation 1 can be rewritten into the Eq. 2:

$$\frac{d\alpha}{dT} = \frac{A}{\beta}e^{-E_a/RT}f(\alpha) \tag{2}$$

where E_a is apparent activation energy, A is pre-exponential factor, R is the gas constant, and α is called reaction degree. The $f(\alpha)$ is a function of α, which reveals the mechanism of reaction. By a series of transforms, thus Eq. 2 can be rewritten as the Eq. 3:

$$\log\beta = [\log\frac{AE_a}{R} - \log g(\alpha) - 2.315] - 0.4567\frac{E_a}{RT} \tag{3}$$

If α is a fixed value, thus $\log g(\alpha)$ is a fixed value, too. The dependence of $\log\beta$ on $1/T$ must give rise to straight line. Thus, reaction activation energy E_a can be obtained from linear slope ($k = -0.4567E_a/R$).

Determination of activation energy and pre-exponential factor by Kissinger method [8]

According to DTA curve and the Kissinger equation (Eq. 4), the activation energy and pre-exponential factor of thermal decomposition reaction of $NH_4NiPO_4{\cdot}6H_2O$ and crystallization of $Ni_2P_2O_7$ can be obtained.

$$\ln\frac{\beta}{T_P^2} = -\frac{E_a}{RT_P} + \ln\frac{AR}{E_a} \tag{4}$$

where β is the heating rate (K min^{-1}), T_P is the peak temperature in DTA curve (K), E_a is the activation energy (kJ mol^{-1}) of thermal process, R is the gas constant (8.314 J mol^{-1} K^{-1}), and A is the pre-exponential factor. The dependence of $\ln(\beta/T_P^2)$on $1/T_P$ must give rise to a straight line. Thus, reaction activation energy E_a can be obtained from linear slope ($k = -E_a/R$), and the pre-exponential factor A can be obtained from linear intercept ($h = \ln(AR/E_a)$).

Determination of thermodynamic parameters of thermal decomposition reaction [9, 10]

The change of the entropy ($\Delta S^{\neq}$) may be calculated according to the Eq. 5:

$$\Delta S^{\neq} = R\ln\left(\frac{Ah}{e\chi k_B T_P}\right) \tag{5}$$

where A is the pre-exponential factor obtained from the Kissinger method, $e = 2.7183$ is the Neper number, χ is the transition factor, which is unity for monomolecular reactions, k_B is the Boltzmann constant (1.381×10^{-23} J K^{-1}), h is the Plank constant (6.626×10^{-34} J s); T_P is

the peak temperature in DTA curve, R is the gas constant (8.314 J mol^{-1} K^{-1}).

The change of the enthalpy ($\Delta H^{\neq}$) may be obtained according to the Eq. 6:

$$\Delta H^{\neq} = E^{\neq} - RT_P \quad (6)$$

where $E^{\neq}$ is the activation energy, E_a, obtained from the Kissinger method. The change of Gibbs free energy $\Delta G^{\neq}$ for the decomposition reaction can be calculated using the well-known thermodynamic Eq. 7:

$$\Delta G^{\neq} = \Delta H^{\neq} - T_P \Delta S^{\neq} \quad (7)$$

Results and discussion

XRD analysis of the product and its calcined samples

Figure 1 shows the XRD patterns of the product dried at 353 K and the products resulting from calcination at different temperatures for 2 h.

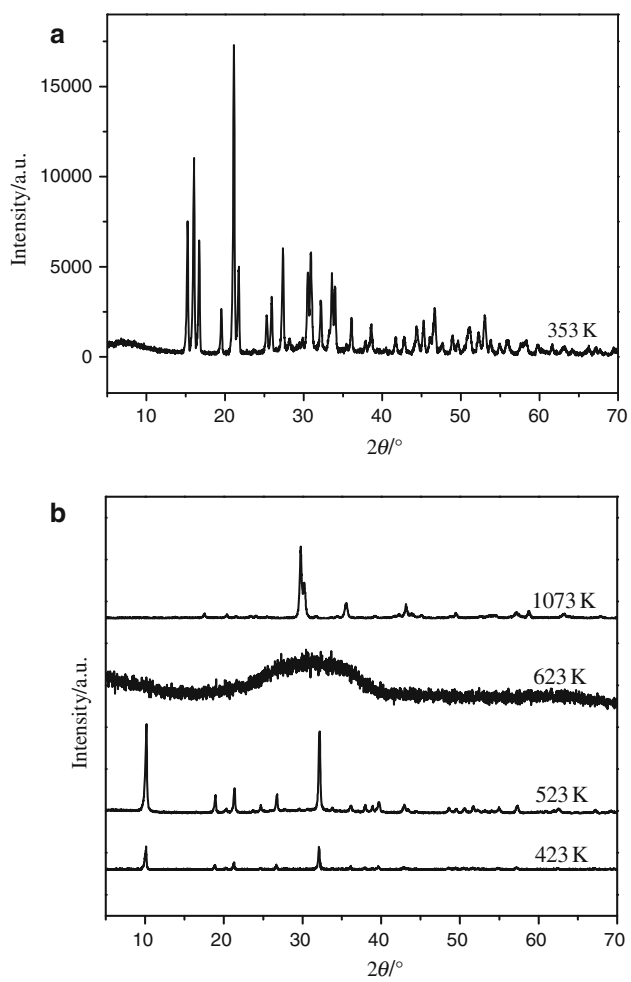

Fig. 1 XRD patterns of the product and its calcined samples at different temperatures for 2 h

From Fig. 1a, the results show that strong intensity and smoothed baseline, a wide and low diffraction pattern of the product is observed, which indicates that the product is crystalline with a higher crystallinity. All the diffraction peaks in the pattern are in agreement with that of orthorhombic $NH_4NiPO_4 \cdot 6H_2O$, with space group Pmm2(25) and cell parameters: $a = 0.6104$ nm, $b = 0.6923$ nm, $c = 1.117$ nm, and $V = 0.4720$ nm^3, from PDF card 21-0034. No diffraction peaks of other impurities, such as $Ni_3(PO_4)_2 \cdot 8H_2O$ and $NH_4NiPO_4 \cdot H_2O$, are observed, which indicates that the single phase $NH_4NiPO_4 \cdot 6H_2O$ are synthesized by solid-state reaction at room temperature. From Fig. 1b, it can be found that two XRD patterns of calcined products at 423 and 523 K are similar, and all the diffraction peaks in the two XRD patterns are found to be in agreement with that of orthorhombic $NH_4NiPO_4 \cdot H_2O$, space group Pmnm(59), from PDF card 50-0425. The strong diffraction peak at about 10.20° for 2θ is attributed to the layered structure of $NH_4NiPO_4 \cdot H_2O$. The interlayer distance of the products from thermal decomposition at temperatures of 423 and 523 K are 0.874 and 0.870 nm, respectively. However, characteristic diffraction peaks of crystalline $NH_4NiPO_4 \cdot H_2O$ disappeared when it was kept at 623 K for 2 h, suggesting that the structure of the crystalline $NH_4NiPO_4 \cdot H_2O$ was destroyed and a new amorphous compound had been formed. When the sample was heated at 1073 K for 2 h, strong intensity and smooth baseline, and a wide and low diffraction pattern of the thermal decomposition product was observed. This indicates that the thermal decomposition product has a high degree of crystallinity. All the diffraction peaks in the pattern are in agreement with that of monoclinic nickel (II) pyrophosphate ($Ni_2P_2O_7$), space group B21/c(14), from PDF card 74-1604.

TG/DTA analysis of the synthetic product

Figure 2 showed the TG/DTA curves of the synthetic product at four different heating rates from ambient temperature to 1073 K, respectively.

The TG/DTA curves show that thermal decomposition of the $NH_4NiPO_4 \cdot 6H_2O$ below 1073 K occurs in two well-defined steps. The first step starts at about 334 K, ends at about 537 K, and characterized by a strong endothermic DTA peak at about 418 K that can be attributed to the five water molecules eliminated from $NH_4NiPO_4 \cdot 6H_2O$ and the formation of $NH_4NiPO_4 \cdot H_2O$. The observed mass loss in the TG curve is 32.11%, which is in good agreement with 32.20% theoretic mass loss of five water molecules eliminated from $NH_4NiPO_4 \cdot 6H_2O$. The second decomposition step begins at about 537 K, and ends at 973 K, which involves an endothermic process with broad DTA peak

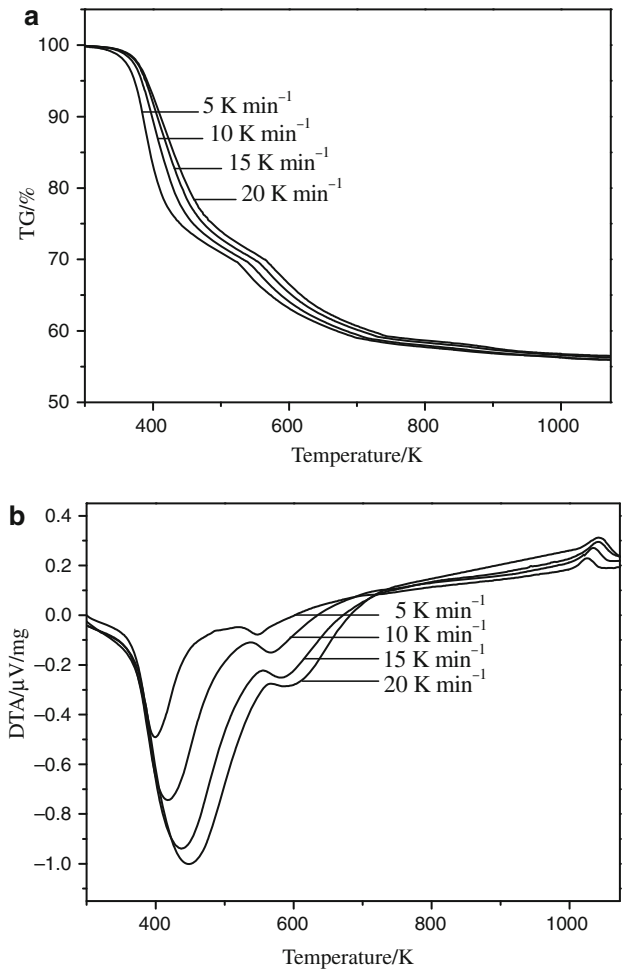

Fig. 2 TG/DTA curves of the $NH_4NiPO_4{\cdot}6H_2O$ at different heating rates

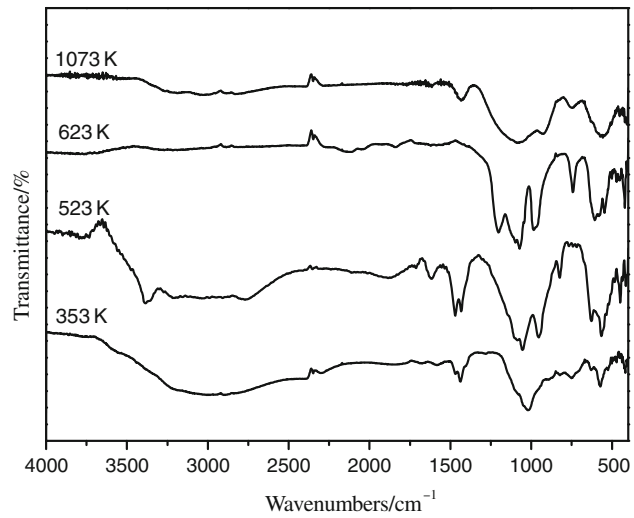

Fig. 3 FT-IR spectra of the product and its calcined samples

at about 568 K, attributed to the decomposition of $NH_4NiPO_4{\cdot}H_2O$ and the formation of $Ni_2P_2O_7$. The corresponding observed mass loss in the TG curve is 14.40 %, which close to 15.73% theoretic mass loss of two ammonia molecules and three water molecules eliminated from two $NH_4NiPO_4{\cdot}H_2O$ molecules. The exothermic DTA peak at about 1035 K can be attributed to the phase change from amorphous $Ni_2P_2O_7$ to monoclinic $Ni_2P_2O_7$.

IR spectroscopic analysis of the product and its calcined samples

FT-IR spectra of the prepared and its calcined samples are shown in Fig. 3. From Fig. 3, the strong bands of the prepared sample at 1013 cm^{-1} is attributed to the P–O stretching vibrations. The bending OPO vibrations appear in the region of 500–630 cm^{-1}. The weak band at about 740 cm^{-1} is the water libration (hindered rotation), while the strong and broad band at about 3000 cm^{-1} is assigned to the stretching OH vibration of the water molecule and the stretching vibration of NH_4^+ [3, 4, 11]. The band at 1432 cm^{-1} can be due to the bending mode of NH_4^+, the weak bands which appear at 1677 and 1579 cm^{-1} in the spectrum of $NH_4NiPO_4{\cdot}6H_2O$ can be ascribed to the bending mode of the HOH [1, 12–14]. The band at 2375 cm^{-1} (OH mode) reveals that the water molecule in $NH_4NiPO_4{\cdot}6H_2O$ forms a weak hydrogen bond, which is in agreement with that of $NH_4NiPO_4{\cdot}6H_2O$ obtained by conventional precipitation method [1, 4], which OH mode in the $NH_4NiPO_4{\cdot}6H_2O$ appear at wavenumbers higher with about 21 cm^{-1} than OH mode of $KMnPO_4{\cdot}H_2O$ obtained by solid-state reaction at room temperature [15]. The deviation cause is not clear. When sample was calcined at 523 K, FT-IR spectra of calcined sample, $NH_4NiPO_4{\cdot}H_2O$, have a little difference in comparison with that of $NH_4NiPO_4{\cdot}6H_2O$. Such as, the band at about 1432 cm^{-1} of $NH_4NiPO_4{\cdot}H_2O$ is split into two bands at 1432 and 1467 cm^{-1}, which is attributed that NH_4^+ tetrahedra present high symmetry in the structure of $NH_4NiPO_4{\cdot}6H_2O$, however, the monohydrated compound take places distortions in the NH_4^+ polyhedra [1]. Besides, the band at 2375 cm^{-1} (OH mode) for $NH_4NiPO_4{\cdot}H_2O$ becomes weaker than that of $NH_4NiPO_4{\cdot}6H_2O$, which can be presumed that hydrogen bond of the water molecule in $NH_4NiPO_4{\cdot}H_2O$ is weaker than that of the water molecule in $NH_4NiPO_4{\cdot}6H_2O$. The intensity of bands at 2300–3500 and 1677 cm^{-1} decrease as the calcination temperature increase, and disappear at 623 K. It is explained by the fact that $NH_4NiPO_4{\cdot}6H_2O$ finish elimination of its six crystal water and an ammonia at 623 K. The band at about 1470 cm^{-1} from calcined sample at 623 K disappears, which indicates the structure of the calcined samples at 623 K takes place during transformation.

SEM analysis of the synthetic product and its calcined samples

The morphology of $NH_4NiPO_4 \cdot 6H_2O$ and its calcined sample are shown in Fig. 4. From Fig. 4a, it can be seen that the $NH_4NiPO_4 \cdot 6H_2O$ sample is composed of platelets. $NH_4NiPO_4 \cdot 6H_2O$ samples illustrated polyhedral grains, which conains particles having a distribution of small particles (150–300 nm) and large particles (300 nm–1.2 μm). From Fig. 4b, $NH_4NiPO_4 \cdot H_2O$ samples obtained at 523 K can still keep platelet morphology of $NH_4NiPO_4 \cdot 6H_2O$. However, thickness of $NH_4NiPO_4 \cdot H_2O$ samples becomes thinner than that of $NH_4NiPO_4 \cdot 6H_2O$ samples. With the increase of calcining temperature, the calcined samples are split into smaller particles further. Figure 4c and d show the SEM micrographs of samples obtained at 973 and 1073 K, respectively. It can be seen that the morphology of two samples have been became near spherical shapes, and there is soft agglomeration phenomenon among one particle of sample. Average particle diameters of samples obtained at 973 and 1073 K are about 70 and 90 nm, respectively.

Activation energy of thermal decomposition of $NH_4NiPO_4 \cdot 6H_2O$ and $Ni_2P_2O_7$ crystallization process

In accordance with TG/DTA analysis and XRD analysis of the synthetic product, and its calcined products mentioned above, thermal process of $NH_4NiPO_4 \cdot 6H_2O$ below 1073 K consists of three steps, which can be expressed as follows:

$$NH_4NiPO_4 \cdot 6H_2O(cr) \rightarrow NH_4NiPO_4 \cdot H_2O(cr) + 5H_2O(g) \quad (9)$$

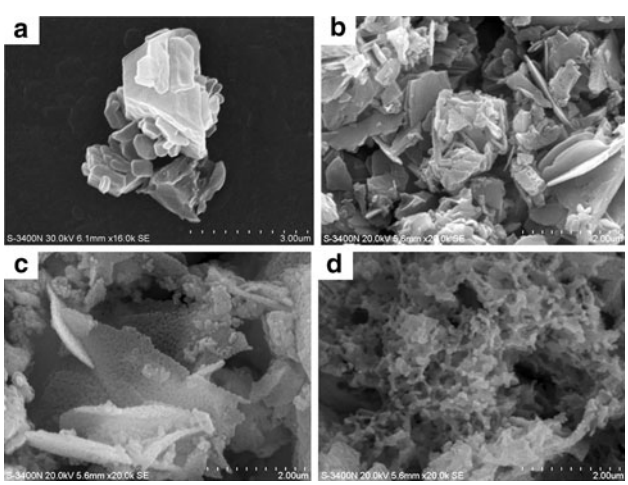

Fig. 4 SEM micrographs of $NH_4NiPO_4 \cdot 6H_2O$ and its calcined samples: **a** 353 K, **b** 523 K, **c** 973 K, **d** 1073 K

$$NH_4NiPO_4 \cdot H_2O(cr) \rightarrow \frac{1}{2}Ni_2P_2O_7(am) + NH_3(g) + \frac{3}{2}H_2O(g) \quad (10)$$

$$Ni_2P_2O_7(am) \rightarrow Ni_2P_2O_7(cr) \quad (11)$$

According to non-isothermal method, the basic data of α and T collected from the TG curves of the thermal decomposition of $NH_4NiPO_4 \cdot 6H_2O$ at various heating rates (5, 10, 15, and 20 K min^{-1}) are illustrated in Tables 1 and 2. According to Eq. 3, the plots of log β versus 1000/T corresponding to different conversions α can be obtained by a linear regression of least-square method, respectively. The FWO analysis results of four TG measurements below 1073 K are shown in Fig. 5. In accordance with FWO equation, the slopes of these straight lines can be determined, then average activation energy for the thermal decomposition reaction of $NH_4NiPO_4 \cdot 6H_2O$ was obtained. Table 3 showed the activation energy and correlation coefficient (r^2) calculated by FWO method for the thermal decomposition steps of $NH_4NiPO_4 \cdot 6H_2O$.

Figure 6 shows Kissinger plots of the thermal process of $NH_4NiPO_4 \cdot 6H_2O$. From the slopes of the straight lines, the activation energy values of three thermal processes of $NH_4NiPO_4 \cdot 6H_2O$ were determined to be 47.81, 90.18, and

Table 1 Correlative data used for drawing plot of log β versus 1000/T for step 1

α	β/K min^{-1}			
	5 (T/K)	10 (T/K)	15 (T/K)	20 (T/K)
0.2	373	387	395	400
0.3	381	396	404	410
0.4	388	404	413	419
0.5	396	413	424	431
0.6	404	423	435	442
0.7	415	434	447	455
0.8	432	451	466	476

Table 2 Correlative data used for drawing plot of log β vs. 1000/T for step 2

α	β/K min^{-1}			
	5 (T/K)	10 (T/K)	15 (T/K)	20 (T/K)
0.2	548	564	578	588
0.3	563	580	594	605
0.4	580	596	613	624
0.5	599	617	633	644
0.6	625	645	661	671
0.7	657	678	695	707
0.8	701	726	745	757

640.09 kJ mol^{-1}, respectively (Table 4). The step 3 exhibits particularly high activation energy value in comparison with the other two steps, which suggests that crystallization of amorphous $Ni_2P_2O_7$ have a slower conversion rate.

From Tables 3 and 4, it is seen that the activation energy values calculated by the FWO method are close to that obtained by Kissinger method, so the results are credible. The relative errors of the slope of the FWO equation straight line for step1 and step 2 are higher than 10%, which implies that E_a values for step 1 and step 2 depend on reaction degree (α). So, we draw a conclusion that the thermal decomposition processes for step 1 and step 2 of $NH_4NiPO_4{\cdot}6H_2O$ could be multi-step reaction mechanisms [10, 16–18].

Thermodynamics of thermal decomposition of $NH_4NiPO_4{\cdot}6H_2O$

Thermodynamic parameters ($\Delta S^{\neq}$, $\Delta H^{\neq}$, and $\Delta G^{\neq}$) were calculated from Eq. 5–7, and the results were shown in Table 5. As can be seen from Table 5, the values of $\Delta S^{\neq}$ for step 1 and step 2 are negative. It means that the corresponding activated complexes have lower disorderness than the initial state. However, the entropy change of the second

Table 3 Activation energies (E_a) and correlation coefficient (r^2) calculated by FWO method

α	Step 1		Step 2	
	E_a/kJ mol^{-1}	r^2	E_a/kJ mol^{-1}	r^2
0.2	59.95	0.9980	87.63	0.9919
0.3	58.93	0.9985	88.72	0.9926
0.4	57.06	0.9983	88.28	0.9835
0.5	53.04	0.9995	93.06	0.9920
0.6	50.84	0.9984	98.92	0.9970
0.7	51.25	0.9994	101.29	0.9955
0.8	50.86	0.9976	102.97	0.9983
Average	54.56 ± 5.39	0.9985	94.41 ± 8.56	0.9930

Table 4 Peak temperature (T_P) and kinetic parameters of thermal process of $NH_4NiPO_4{\cdot}6H_2O$ obtained from Kissinger method

	Step 1	Step 2	Step 3
T_P (K) in four heating rates/K min^{-1}			
5	405	552	1025
10	425	569	1035
15	434	582	1041
20	443	589	1043
E_a/kJ mol^{-1}	47.81	90.18	640.09
ln$A$	12.44	17.94	74.09
r^2	0.9973	0.9950	0.9888

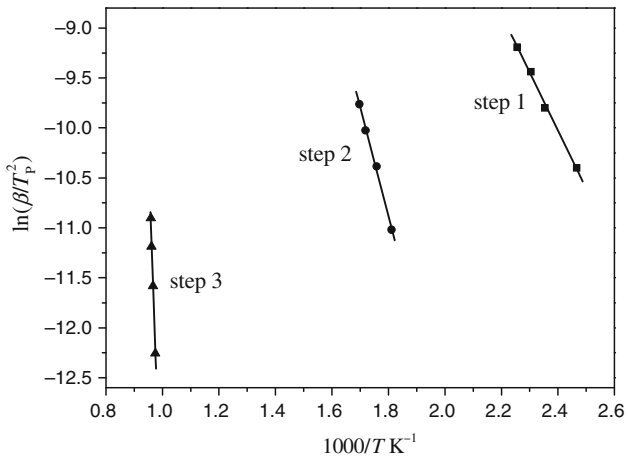

Fig. 6 Kissinger plots of the thermal process of $NH_4NiPO_4{\cdot}6H_2O$

Table 5 Thermodynamic parameters of the decomposition reaction of $NH_4NiPO_4{\cdot}6H_2O$

Parameters	Step 1	Step 2
$\Delta S^{\neq}$/J mol^{-1} K^{-1}	−153.09	−107.05
$\Delta H^{\neq}$/kJ mol^{-1}	44.13	85.28
$\Delta G^{\neq}$/kJ mol^{-1}	111.95	148.33

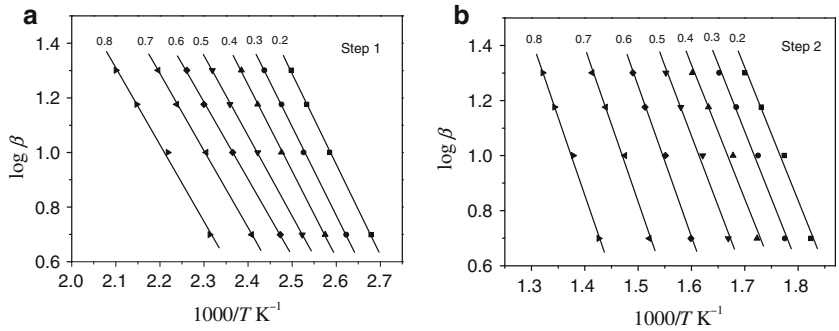

Fig. 5 FWO analysis for the thermal decomposition of $NH_4NiPO_4{\cdot}6H_2O$

activated complex was higher than that of the preceding one. In the terms of the theory of activated complex (transition theory), the step 1 of the thermal decomposition of $NH_4NiPO_4 \cdot 6H_2O$ may be interpreted as a ''slow'' stage, while the step 2—as a "fast" stage [10, 19, 20]. The positive values of $\Delta G^{\neq}$ at all studied steps are due to the fact that dehydration of the crystal waters of $NH_4NiPO_4 \cdot 6H_2O$, deamination, and intramolecular dehydration of the protonated phosphate group from $NiHPO_4$ are not spontaneous at room temperature. The larger $\Delta G^{\neq}$, the harder decomposition process. So, the second decomposition process (step 2) occur harder than the first decomposition process (step 1). The endothermic peaks in DTA curve agree well with the positive sign of the activation enthalpy ($\Delta H^{\neq}$). The value of $\Delta H^{\neq}$ of the second decomposition process was larger than that of the first decomposition process, which means that the second decomposition process needs more energies than the first decomposition process.

Conclusions

This research has successfully achieved a simple room temperature synthesis of single phase $NH_4NiPO_4 \cdot 6H_2O$. XRD analysis suggested the formation of binary phosphates of orthorhombic $NH_4NiPO_4 \cdot 6H_2O$, and its decomposition product $NH_4NiPO_4 \cdot H_2O$ with layered structure. The thermal process of $NH_4NiPO_4 \cdot 6H_2O$ in the range of ambient temperature—1073 K is a complex process, which involve the dehydration of the five crystal water molecules at first, and then deamination, dehydration of the one crystal water molecule, intramolecular dehydration of the protonated phosphate groups to form amorphous $Ni_2P_2O_7$ together, and at last crystallization of $Ni_2P_2O_7$. The kinetics of the thermal decomposition of $NH_4NiPO_4 \cdot 6H_2O$ was studied using non-isothermal TG technique applying model-fitting method. The average values of the activation energies associated with the $NH_4NiPO_4 \cdot 6H_2O$ thermal decomposition and crystallization of $Ni_2P_2O_7$ were 47.81, 90.18, and 640.09 kJ mol^{-1}, respectively. Dehydration of the five crystal water molecules of $NH_4NiPO_4 \cdot 6H_2O$, and deamination, dehydration of the crystal water of $NH_4NiPO_4 \cdot H_2O$, intramolecular dehydration of the protonated phosphate group from $NiHPO_4$ together could be multi-step reaction mechanisms. The thermodynamic parameters ($\Delta S^{\neq}$, $\Delta H^{\neq}$, and $\Delta G^{\neq}$) of the decomposition reaction of $NH_4NiPO_4 \cdot 6H_2O$ are obtained. These data will be important for further studies of the studied compound, and to solve various scientific and practical problems involving the participation of solid phases.

Acknowledgements This study was financially supported by the Guangxi Natural Scientific Foundation of China (Grant No. 0832111), and the Guangxi Science and Technology Agency Research Item of China (Grant No. 0895002–9).

References

1. Goñi A, Pizarro JL, Lezama LM, Barberis GE, Arriortua MI, Rojo T. Synthesis, crystal structure and spectroscopic properties of the $NH_4NiPO_4 \cdot nH_2O$ ($n = 1$, 6) compounds; magnetic behaviour of the monohydrated phase. J Mater Chem. 1996;6:421–7.
2. Li YF, Cui W, Zhu GS, Qiu SL, Fang QR, Wang CL. Hydrothermal synthesis and characterization of $Ni_3(PO_4)_2 \cdot 8H_2O$ with 8-ring and 4-ring network structure. Chem J Chin Univ. 2002;23:1480–2.
3. Wu WW, Fan YJ, Wu XH, Liao S, Li SS. Preparation via solid-state reaction at room temperature and characterization of layered nanocrystalline $NH_4MnPO_4 \cdot H_2O$. J Phys Chem Solids. 2009;70:584–7.
4. Koleva VG. Metal–water interactions and hydrogen bonding in dittmarite-type compounds $M'M''PO_4 \cdot H_2O$($M' = K^+$, NH_4^+; $M'' = Mn^{2+}$, Co^{2+}, Ni^{2+})—Correlations of IR spectroscopic and structural data. Spectrochim Acta A. 2005;62:1196–202.
5. Carling SG, Day P, Visser D. Crystal and magnetic structures of layer transition metal phosphate hydrates. Inorg Chem. 1995;34:3917–27.
6. Flynn JH, Wall LA. A quick direct method for the determination of activation energy from thermogravimetric data. Polym Lett. 1966;4:323–8.
7. Ozawa TA. New method of analyzing thermogravimetric data. Bull Chem Soc Jpn. 1965;38:1881–6.
8. Kissinger HE. Reaction kinetics in differential thermal analysis. Anal Chem. 1957;29:1702–6.
9. Boonchom B, Puttawong S. Thermodynamics and kinetics of the dehydration reaction of $FePO_4 \cdot 2H_2O$. Phys B. 2010;405:2350–5.
10. Vlaev L, Nedelchev N, Gyurova K, Zagorcheva M. A comparative study of non-isothermal kinetics of decomposition of calcium oxalate monohydrate. J Anal Appl Pyrol. 2008;81:253–62.
11. Rajić N, Ristić A, Kaučič V. On the possibility of the preparation open framework manganese phosphate. Zeolites. 1996;17:304–9.
12. Boonchom B, Danvirutai C, Santi Maensiri S. Soft solution synthesis, non-isothermal decomposition kinetics and characterization of manganese dihydrogen phosphate dihydrate $Mn(H_2PO_4)_2 \cdot 2H_2O$ and its thermal transformation. Mater Chem Phys. 2008;109:404–10.
13. Onoda H, Sugino N, Kojima K, Nariai H. Mechanochemical effects on synthesis and properties of manganese–neodymium diphosphates. Mater Chem Phys. 2003;82:831–6.
14. Šoptrajanov B, Jovanovski G, Pejov L. Very low H–O–H bending frequencies. III. Fourier transform infrared study of cobalt potassium phosphate monohydrate and manganese potassium phosphate monohydrate. J Mol Struct. 2002;613:47–54.
15. Wu XX, Wu WW, Liao S, Fan YJ, Li SS. Preparation via solid-state reaction at room temperature and characterization of layered nanocrystalline $KMnPO_4 \cdot H_2O$. J Alloys Compd. 2009;479:541–4.
16. Genieva SD, Vlaev LT, Atanassov AN. Study of the thermo-oxidative degradation kinetics of poly(tetrafluoroethene) using iso-conversional calculation procedure. J Therm Anal Calorim. 2010;99:551–61.
17. Budrugeac P, Muşat V, Segal E. Non-isothermal kinetic study on the decomposition of Zn acetate-based sol-gel precursor. J Therm Anal Calorim. 2007;88:699–702.

18. Boonchom B, Danvirutai C. Kinetics and thermodynamics of thermal decomposition of synthetic $AlPO_4 \cdot 2H_2O$. J Therm Anal Calorim. 2009;98:771–7.
19. Boonchom B. Kinetics and thermodynamic properties of the thermal decomposition of manganese dihydrogenphosphate dihydrate. J Chem Eng Data. 2008;53:1533–8.
20. Danvirutai C, Noisong P, Youngme S. Some thermodynamic functions and kinetics of thermal decomposition of $NH_4MnPO_4 \cdot H_2O$ in nitrogen atmosphere. J Therm Anal Calorim. 2010;100:117–24.